Aerospace Science and Technology 74 (2018) 72–80

Contents lists available at ScienceDirect

Aerospace Science and Technology

www.elsevier.com/locate/aescte

Effect of cowl shock on restart characteristics of simple ramp type hypersonic inlets with thin boundary layers

Lianjie Yue [a,*], Yinan Jia [a,b], Xiao Xu [a], Xinyu Zhang [a,b], Peng Zhang [c]

[a] Institute of Mechanics, Chinese Academy of Sciences, No. 15 Beisihuanxi Road, Beijing 100190, China
[b] School of Engineering Science, University of Chinese Academy of Sciences, Beijing 100049, China
[c] Department of Mechanical Engineering, The Hong Kong Polytechnic University, Hung Hom, Hong Kong

ARTICLE INFO

Article history:
Received 9 June 2017
Received in revised form 6 December 2017
Accepted 22 December 2017
Available online 31 January 2018

Keywords:
Inlet restart
Cowl shock
Shock wave boundary layer interactions

ABSTRACT

The effect of cowl angle on the restart characteristics of simple ramp type hypersonic inlets was experimentally investigated in shock tunnel equipped with schlieren imagery and static pressure measurement. The cowl shock strength is found to be a key factor that determines the inlet restart and makes the restart contraction ratios significantly deviate from the Kantrowitz criterion. Stronger cowl shock tends to degrade the inlet restart capability by causing larger separation bubble and higher pressure loss during the restarting process. In particular, a sensitive range of the cowl angles, within which the restart contraction ratio decreases rapidly, was identified. A design concept of multiple noncoalesced cowl shocks was thus proposed and proven to significantly improve the inlet restart capability.

1. Introduction

Hypersonic inlets use a combination of external and internal compression, which adds complexity in the inlet starting, especially for the fixed-geometry configurations. The inlet has the risk of becoming unstarted at low flight Mach number, or large angle of attack, or high back pressure rising in the combustor [1,2]. Mahapatra and Jagadeesh [3] and Chang et al. [4] even found so-called local unstart at high Mach number. The inlet restart capability is therefore crucial for efficient operations of hypersonic aircraft. Numerous studies have been conducted to investigate the inlet restart (or self-starting) characteristics.

In the early studies [5,6], Kantrowitz proposed a theoretical model for supersonic inlet restart based on the assumptions that a normal shock wave stands at the cowl lip station and the quasi-steady, one-dimensional, isentropic internal flow has a sonic condition at the inlet throat. The maximum allowable internal contraction ratio was consequently derived as a function of the inflow Mach number. Mölder et al. [7], Najafiyazdi et al. [8] and Veillard et al. [9] further studied the limiting contractions for restarting scramjet inlets with overboard spillage or wall perforations based on the Kantrowitz theory. Although the theory provides a basic criterion for inlet design, the hypersonic inlet starting process, involving complex shock patterns accompanied with a large scale boundary layer separation, is significantly different from the simplified assumption of swallowing a normal shock. A number of experiments have verified that the inlet can restart at internal contraction ratios beyond the Kantrowitz limit [10,11], and a significant scatter in the restart contraction ratios has been observed [10,12]. These indicate that the Kantrowitz theory is not applicable to hypersonic inlets because of the oversimplified assumptions mentioned above. The restart problem should be attributed, at least in part, to the shock–boundary layer interaction in the region of the cowl leading-edge station, and it has strong relations with other factors besides Mach number.

Taking the actual viscous flow into account, Goldberg and Hefner [13,14] studied the restart capability of a simplified two-dimensional inlet with thick boundary layers relative to the inlet height at Mach 6.0. The dependence of restart contraction ratios on the inlet geometries, the relative boundary layer thickness, and the wall-to-freestream temperature ratio were preliminarily surveyed. The inlet cowl angle is found to have a favorable effect on the inlet restart, which contradicts with our conventional understanding. In fact, it is noted that the results were simultaneously coupled with the variation of relative thickness of boundary layers.

McGregor et al. [15] investigated the starting process for planar inlets in a gun tunnel at Mach 8.3 for various contraction ratios, Reynolds numbers and initial tunnel pressures. The inlet starting is promoted by lowering the pre-start back pressure in the tunnel, by decreasing the contraction area ratio, and by decreasing the cowl angle.

* Corresponding author.
E-mail address: yuelj@imech.ac.cn (L. Yue).

https://doi.org/10.1016/j.ast.2017.12.018
1270-9638/

Van Wie et al. [16] further investigated the unstart/restart characteristics of a small-scale rectangular inlet at Mach 3.0 and observed two types of unstart/restart behavior, which are classified as “hard” or “soft” based on the occurrence of hysteresis. Although a crude boundary between the soft and hard modes was drawn in the parameter space of cowl length and cowl height, their transition criterion needs to be further clarified. It is likely to be related to the cowl angle because the restart contraction ratio corresponds to a specific cowl angle at given cowl length and height.

Flock and Gülhan [17] experimentally studied the restart behavior of a three-dimensional scramjet inlet and found that exchanging the V-shaped cowl with a straight-cowl geometry improved inlet starting with the additional mass spillage. In recent years, increasing attentions have been paid to developing various methods of promoting the inlet starting. Chang et al. [18,19] studied the effects of bleeding on unstart/restart characteristics of hypersonic inlets and found the bleeding can reduce the starting Mach number. Tahir and Mölder [20] and Ogawa et al. [21] proposed a method by taking advantage of highly unsteady effect. Variable geometry techniques were also investigated extensively for inlet starting [22,23].

In spite of aforementioned advances in understanding hypersonic inlet restart, the roles of cowl shock have not been adequately clarified and a general design rule for improving the inlet restart has not been established. Specifically, cowl shock was found to have some effects on the inlet restart, but to our knowledge, details of how it affects the inlet restart are not available, particularly when decoupled from other factors. The present study was motivated to elucidate the influence of the cowl shock on the restart characteristics. Simple ramp type inlet models were designed for facilitating the focus on the cowl shock effects. Thin boundary layers were considered in the present study because they occupy less than one fourth of the cowl lip height in the hypersonic inlets.

2. Experimental setup

2.1. Wind tunnel and test conditions

The present experiments were conducted in the GJF shock tunnel of Institute of Mechanics, Chinese Academy of Sciences. The shock tunnel, operating at equilibrium interface condition, is equipped with an 11.2 m-long driver section and a 22 m-long driven section filled with compressed air, followed by an axisymmetric nozzle, test section and vacuum tank, as shown in Fig. 1. The test chamber is fully closed with two embedded glass windows (350 mm in diameter) for optical access. In the present experiments, the nozzle Mach number M_∞ was 4.0, the static pressure p_∞ is 9.0 kPa, the total temperature T_0 is 430 K, and the unit Reynolds number $\mathrm{Re}_{\infty,m}$ is 3.58×10^7/m. A typical test duration is about 25 ms, as shown in Fig. 2, in which $t = 0$ indicates the time instant when the pressure sampling was triggered by the pressure transducer in the upstream of the nozzle.

2.2. Technique for inlet restart test

To examine the hypersonic inlet restart characteristics within the short duration of the shock tunnel, a newly proposed test method [24], which has been validated against the experimental data from blow down tunnels, was adopted in the present study, as shown in Fig. 3. A Terylene diaphragm is placed at the inlet exit with a coherent electric resistance wire on its leeward insulated from the shock tunnel and inlet model. At the beginning, the inlet is choked into big buzz due to the obstruction of the diaphragm. Concurrently, the voltage signal from the total pressure transducer triggers the delay-time signal generator, which in turn generates a pulse voltage signal after a specified delay of 40 ms to actuate

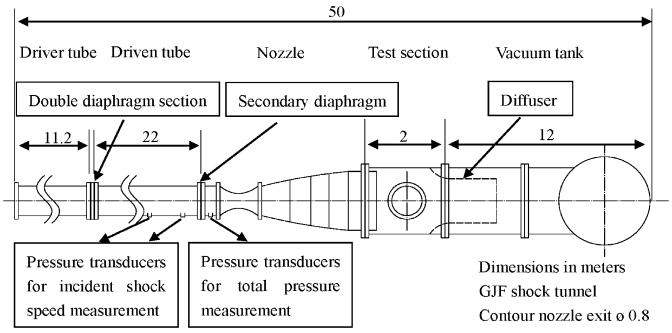

Fig. 1. Sketch of the GJF shock tunnel (unit: m).

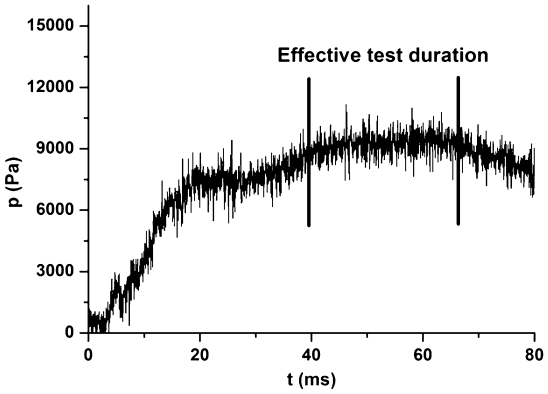

Fig. 2. A typical static pressure–time history at the nozzle exit.

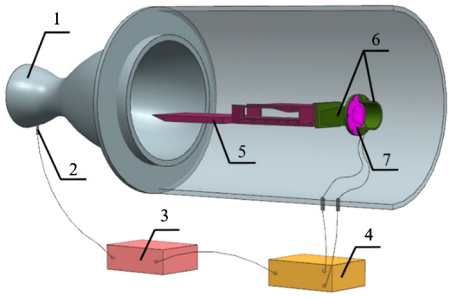

Fig. 3. Schematic of the experimental devices for inlet restart in shock tunnel. 1. Shock tunnel nozzle, 2. Pressure probe, 3. Delay time signal generator, 4. Electrical igniter, 5. Inlet model, 6. Device for diaphragm installation, 7. Terylene diaphragm.

the high-voltage igniter. The diaphragm is subsequently ruptured within a few milliseconds due to the heating of the electric resistance wire. It is noted that the delay time is specified so that the diaphragm rupture occurs within the effective shock tunnel duration after the establishment of periodic unstarted flow in the inlet. Similar to that of conventional wind tunnels, the inlet restarting process can be investigated to check its restart capability after the disappearance of the choke.

2.3. Simplified inlet model

As with Refs. [10,13,14], a simplified inlet model, as shown in Fig. 4(a), was tested in the present investigation to gain an in-depth understanding, which would be applicable to realistic hypersonic inlets. The model has a constant span width of 80 mm, five different wedge angles $\alpha = 7°$, 8°, 9°, 11° and 15° for varying the cowl shock strength, and two different cowl lip heights H are designed as 30 mm and 40 mm. The boundary layer thickness at the cowl lip station is directly related to the bottom plate length in the upstream of the cowl lip, which is designed as $L = 200$ mm,

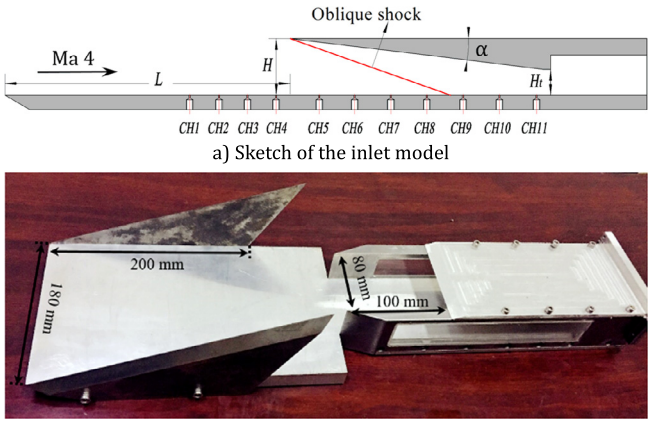

a) Sketch of the inlet model

b) Photograph of the inlet model (L=400 mm, H=40 mm)

Fig. 4. (a) Schematic and (b) photograph of the test inlet model.

300 mm and 400 mm. The bottom plate upstream the sidewall is 180 mm in width. For the inlet models with $L = 300$ mm and 400 mm, side-wings of 200 mm length are further assembled to the bottom plate to help prevent the side flow interference. The inlet restart capability is represented by maximum internal contraction ratio (ICR, defined as H/H_t) allowing inlet restart. For a fixed combination of the cowl angle α, the cowl lip height H, and the plate length L, a set of cowl plates with different throat height H_t were tested. ICR was adjusted by less than 0.05 in each test for determining its maximum value with good accuracy.

The inlet model was equipped with 11 static pressure ports along the centerline of the bottom wall and with separation distance of either 20 or 25 mm. Dynamic pressure transducers, marked CH1–CH11 (CH4 port always located at 10 mm upstream the cowl lip station), were installed directly on the model wall so that the internal cavum and the conduit do not degrade the actual frequency response significantly. The transducers have a range of 200 kPa for CH1–CH8 and 500 kPa for CH9–CH11, with an uncertainty of 0.3% in the full range and with the natural response frequency of 30 kHz. A 128-channel data acquisition system, consisting of voltage signal amplifiers and the National Instruments DAQ PXI-6150 cards, was used for pressure measurement with the sampling frequency of 31.2 kHz per channel.

To visualize the internal flow field, two windows with silica glasses were installed on the sidewalls for optical access. Fig. 4(b) presents a photograph of the inlet model with one sidewall removed for clarity. The present schlieren imagery adopts a 'Z-type' schlieren imaging arrangement, a xenon lamp as a continuous light source, two 350 mm diameter spherical mirrors, and a high-framing rate CMOS camera (Photron FASTCAM SA4) equipped with a 200 mm $f/2.8$lens (Nikon Nikkor). The sampling rate of the schlieren visualization was set at 5000 frames per second. The camera was shuttered to 6.2 μs and the image resolution is 896×896 pixels.

3. Results and discussion

3.1. The ratio of cowl lip height to the boundary layer thickness

The boundary layer thickness δ was measured with pitot tube at different flat plate locations. Fig. 5(a) illustrates the velocity profiles at three streamwise locations $L = 200$ mm, 300 mm and 400 mm. The boundary layer thickness is 2.4 mm, 4.5 mm, 6.6 mm, respectively. For all the experimental cases in the present study, the ratio of H/δ ranges approximately from 4.5 to 16.7, as shown in Fig. 5(b). This means a thin boundary layer relative to the cowl lip height, in contrast with Goldberg's experiments [13,14].

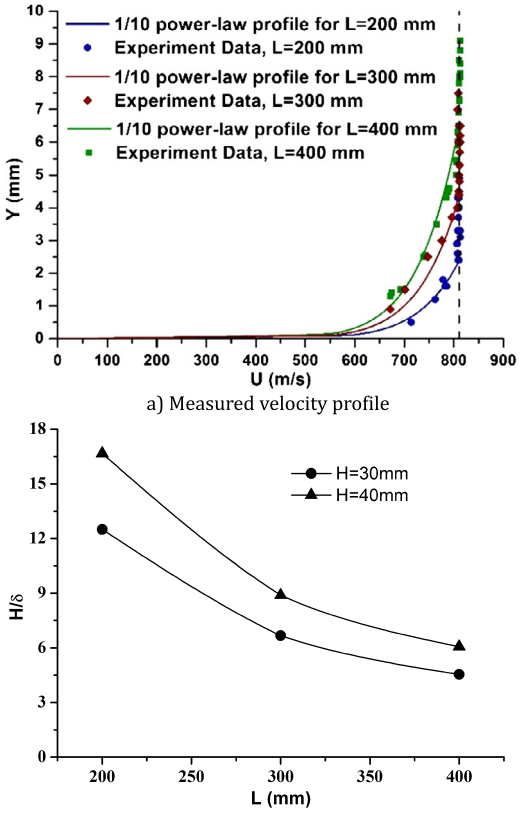

a) Measured velocity profile

b) Ratio of cowl lip height to boundary layer thickness

Fig. 5. Flat plate boundary layer thickness measurement.

3.2. Inlet unstart/restart behaviors and transitional phenomenon

Fig. 6 shows typical schlieren images at $H = 40$ mm, $L = 400$ mm, $\alpha = 9°$ for various ICR of 1.35, 1.55 and 1.65 during the inlet unstart/restart process. The corresponding pressure–time histories at CH4 are shown in Fig. 7, where the pressure is normalized by freestream static pressure p_∞. As a benchmark case, the pressure curve of started inlet without diaphragm is also shown in Fig. 7 for comparison. Similar to the observations of Tan et al. [25,26] for unstart phenomena caused by downstream throttling in a blow down tunnel, a big buzz firstly occurs on the pressure–time curves of all models with diaphragm with frequencies around 100 Hz, which depends on the volume of the inlet internal passage [25]. A separation bubble and its induced shock oscillation can be observed from $t = 30$ ms to 40 ms in Fig. 6. The separation shock approaching the cowl lip at $t = 30$ ms corresponds to a pressure peak in the internal passage, which subsequently pushes the shock to move upstream till outside the optical window at $t = 35$ ms. This indicates that periodic unstarted flow has been established, which is prerequisite for the restart tests.

After the high-voltage igniter is actuated at $t = 40$ ms, the diaphragm ruptures gradually in a few milliseconds. As the expansion waves propagate upstream, the separation bubble moves downstream and shrinks continually in the internal passage for the inlet model with ICR = 1.35, as shown in Fig. 6(a). The separation bubble finally vanishes and a stable flow is established in the internal contraction section. Inlet restart is achieved and the pressure drops to the same level as that without diaphragm, as shown in Fig. 7. However, the inlet cannot restart for the model with ICR = 1.65, as shown in Fig. 6(c). The separation bubble and the accompanied shock move downstream to pass the cowl lip at $t = 50$ ms, and subsequently move upstream due to the choke downstream. The shock finally stands at the upstream of the cowl lip, oscillates

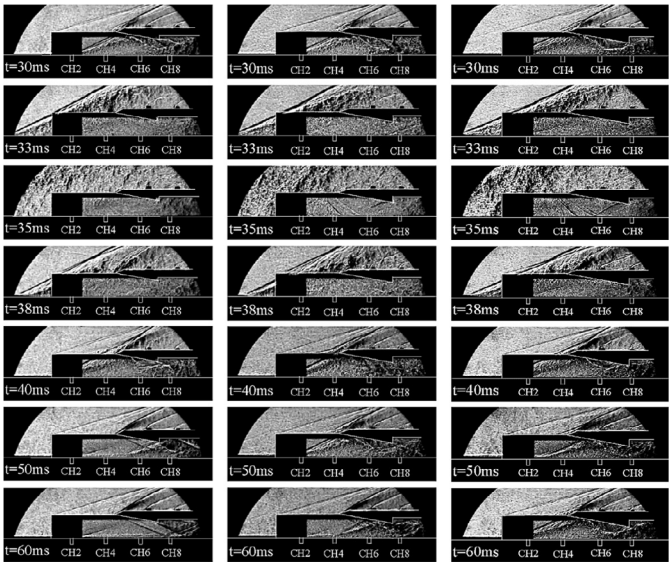

a) ICR=1.35 (restarted) b) ICR=1.55 (transitional) c) ICR=1.65 (un-restarted)

Fig. 6. Schlieren images during inlet unstart/restart process ($H = 40$ mm, $L = 400$ mm, $\alpha = 9°$).

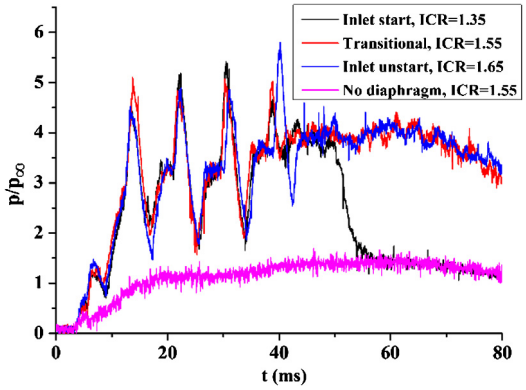

Fig. 7. Static pressure–time histories for different ICR of 1.35, 1.55 and 1.65 at CH4 ($H = 40$ mm, $L = 400$ mm, $\alpha = 9°$).

with a small magnitude, and results in high pressures at CH4 different from the restarted inlet of ICR = 1.35.

A transitional case is shown in Fig. 6(b), where ICR = 1.55. Similar to the typical un-restarted inlet flow pattern shown in Fig. 6(c), the separation-induced shock does not pass through the throat. However, the shock finally stands in the internal contraction section and impinges on the cowl at $t = 60$ ms, implying that the inlet mass capture may be the same as the started inlet. According to the conventional definition of the inlet starting [10], this flow pattern should be deemed as started since the flow characteristics in the internal portion of the inlet do not alter the capture characteristics. However, the inlet characterizes a large separation bubble with an induced shock, which does not take place as in the normal started mode. As a result, the pressure at CH4 remains as high as that of the un-restarted case. Owing to the loss in the separation bubble and the separation shock in the transitional mode, the inlet cannot take in sufficient air with high total pressure to work properly in the combustor. So the transitional mode should not be considered as a restarted one. Its mechanism merits further studies in view of the flow complexity. The restarted mode is identified in the present experiments as the case in which all pressures and schlieren images are the same as those without diaphragm.

3.3. Effects of cowl shock strength on inlet restart

Fig. 8 shows the variation of maximum ICR with the plate lengths L at the cowl lip height H of 30 mm or 40 mm for various cowl angles. It is noted that, for any cowl angle, the restart ICR limit maintains nearly fixed at different plate lengths and cowl lip heights. The thin boundary layer in the present experiments (H/δ ranges from 4.5 to 16.7) exerts minor influence on the inlet restart capability. This is different from Goldberg's experiments [14], in which thicker boundary layer would degrade the inlet restart capability when H/δ is less than 2.0.

The inlet total-pressure recovery, taking into account of both shock and viscous losses, is the governing factor determining the inlet starting. Thin boundary layers contribute almost equally because they merely occupy considerably small portion of the inlet. On the other hand, the separation-induced shock patterns remain approximately the same for the tested cases. The separation shock angles around the cowl lip are found to be about 24°, as shown in Fig. 6. The free interaction theory proposed by Chapman et al. [27] for boundary layer separation in supersonic flows has been experimentally validated in unstarted hypersonic inlet flow by Wang et al. [28]. It was suggested that the flow properties in the vicinity of the separation point depend on the local skin-friction coefficient and the Mach number. For a moderate range of Reynolds number of $3 \times 10^4 < \mathrm{Re}_\delta < 1.2 \times 10^6$, the gross features of the separated region become independent of the Reynolds number, and a correlation for the pressure ratio, p_s/p_∞, between the separation and freestream flow was suggested by Zukoski [29] as $p_s/p_\infty = 1 + 0.5\ M_\infty$. Consequently, the separation shock patterns are similar at a fixed Mach number. By using the Rankine–Hugoniot relation, the correlation at Mach number 4.0 yields a 24.3° separation-shock angle, which is in a good agreement with the observed 24° from the schlieren images. To sum up, the similar

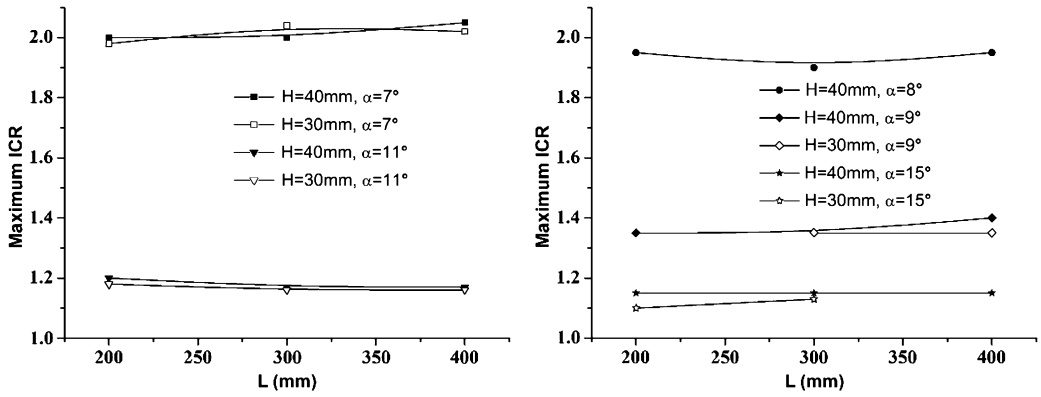

Fig. 8. Variation of the maximum ICR with the plate length for various cowl lip heights and cowl angles.

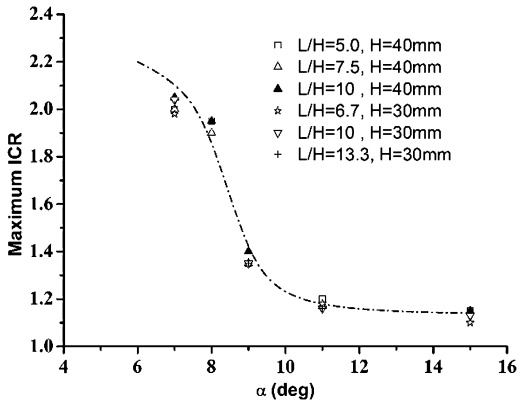

Fig. 9. Variation of the maximum ICR with the cowl angle for various L/H.

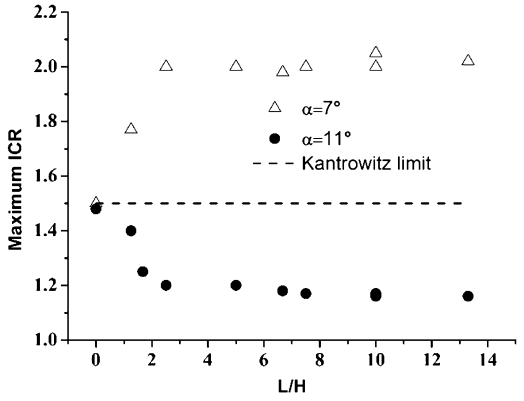

Fig. 10. Variation of maximum ICR with L/H at the cowl angle of 7° and 11°.

shock patterns and relatively thin boundary layers result in approximately constant ICR limits for various plate lengths and cowl lip heights.

Fig. 9 shows the variation of the maximum ICR allowing inlet restart with the cowl angle α for various plate length L and cowl lip heights H, where L/H is specified as a nondimensional parameter. It is noted that the maximum restart ICR decreases as the cowl angle increases. The boundary layer separation in the vicinity of the cowl lip station, which is related to the cowl shock, may play an important role in starting characterization. The increasing cowl angle results in a larger separation bubble and a smaller aerodynamic throat for inlet starting in the internal contraction section. In addition, the higher loss in the total pressure caused by the stronger cowl shock weakens the capability of the flow passing through the throat. Consequently, the maximum ICR allowing for inlet restart must decrease to accommodate to these changes. Furthermore, a remarkable change in the maximum ICR can be seen within the cowl angle range of 7°–9°, where the maximum ICR drops sharply. This phenomenon is notable because of its importance for designing the inlet configuration, and its mechanism shall be explained shortly in the next section. Beyond the cowl angle of 11°, the inlet restart ICR shows slight dependence on the cowl shock. One possible reason is that the influence of further increase in the cowl shock strength becomes moderate because the maximum ICR is sufficiently small (less than 1.2). From these results, we can infer that the cowl shock effect is likely to be the cause of significant scatter in the restart contraction ratios.

The cowl shock exhibits a dominant influence on restart contraction ratio at relative boundary layer thickness δ/H from 6.0% to 22.0% (L/H from 4 to 13.3). As to the limit of thin boundary layer, the Kantrowitz theory is satisfied for inviscid flow, in which the cowl shock would not have effects on the inlet restart. We also supplemented some experiments with the plate length L of 100 mm, 50 mm and 0 mm for the cowl angles of 7° and 11°. The restart ICR limits are plotted in Fig. 10 against L/H. A significant change in the maximum ICR occurs for $L/H < 2.5$, where the maximum ICR approaches the Kantrowitz limit 1.50 as L/H decreases to 0.

Based on the free interaction theory, the separation shock stands on the plate at shock angle of about 24°. Therefore, the bottom plate length must be at least 2.2 ($= \cot(24°)$) times of the cowl lip height to maintain the separation shock pattern when it passes through the cowl lip. For $L/H < 2.2$, the change in separation shock pattern and its associated separation bubble, as shown in Fig. 11, contributes to different maximum ICRs from large L/H. Normal shock can be observed in the case of zero plate length ($L/H = 0$), which accords with Kantrowitz's assumption. It can therefore be deduced that the difference in the maximum ICR varying with the cowl angle reduces gradually as L/H approaches 0, and eventually diminishes at vanishing boundary layer thickness. Nevertheless, we are concerned with the cases with relative boundary layer thickness δ/H from 6.0% to 22.0% because they are relevant to those in most hypersonic inlets.

3.4. Mechanism of sudden decline in restart capability

In order to facilitate the analysis on sudden change of maximum ICR in Fig. 9, numerical simulation was conducted for representative cases. Commercial code CFD++ were used to solve the compressible two-dimensional Navier–Stokes equations. The turbulence model of k–ω SST was employed with a compressibility correction for high Mach number flows. The convection terms of the governing equations were discretized with a second-order TVD method based on a new multi-dimensional interpolation framework. An approximate Riemann solver named Harten–Lax–van Leer contact (HLLC) was used to define interface fluxes based on local wave-model solutions. The minmod limiter was employed to suppress spurious oscillations near the discontinuities while high-order accuracy is retained in the regions away from the discontinuities. The unsteady terms were discretized with a second-order fully implicit scheme. In addition, the multi-grid and dual time-step methods were employed to accelerate convergence. Previous studies have shown that the solver can efficiently resolve high Mach number flows [30,31].

Fig. 12 shows the computational domain and hybrid mesh used in the present simulations. The experimental nozzle condition is specified at the inflow boundary and all variables are extrapolated at the outlet boundary. Far field condition is applied at the upper and lower boundaries. At the solid walls, no-slip and isothermal condition ($T_w = 300$ K) are imposed. The diaphragm is specified as solid wall before its rupture. The diaphragm rupture is modeled by replacing the wall boundary condition with a low back

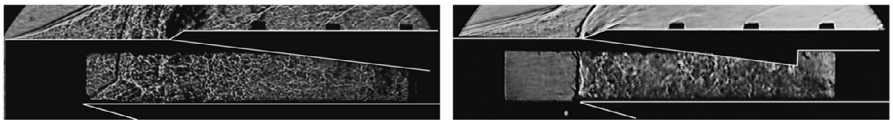

a) H=40 mm, L=50 mm and α=7° b) H=40 mm, L=0 mm and α=7°

Fig. 11. Schlieren image for the inlet with small L/H during inlet starting process.

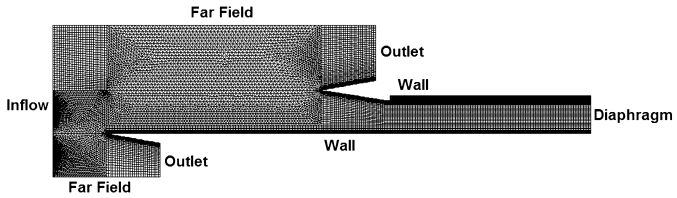

Fig. 12. Computational domain, mesh grids and boundary conditions for the simulation of hypersonic inlets. A coarser mesh of 0.03 million grid points is shown for clarity.

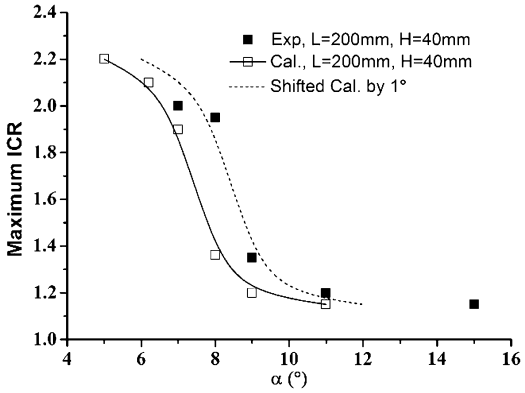

Fig. 13. Comparison between numerical and experimental results.

pressure imposition. The transient flow fields are computed with a time step of 0.1 μs and are converged at every global time step by inner iterations of up to 50 steps. The first mesh size normal to the wall is 1 μm, corresponding to $y^+ < 1$ on the solid surface. The total number of mesh grids is about 0.1 million.

Taking the inlet configurations with cowl lip height H of 40 mm and the plate length L of 200 mm as a representative case, we attempted to explain the rapid change of the maximum ICR with the cowl angle from 7° to 9° by numerical results. The simulation was first validated by comparison with the experimental maximum ICRs for different cowl angles. Fig. 13 shows that numerical results well capture the trend of the maximum ICR varying with the cowl angle. Although the quantitative agreement is less satisfactory as the numerical predictions are moderately smaller than the experimental ICR, it is interesting to observe that a good agreement can be obtained if the numerical results were right shifted by 1°. This implies that the present simulation overestimates the size of the separation bubble and therefore underestimates the effective height of flow passage, which in turn results in a smaller maximum ICR.

Fig. 14 shows the numerical Mach number contours of two un-restarted inlets with the cowl angles of 7° and 9°, respectively, with ICRs slightly larger than the corresponding numerical maximum ICRs. For these configurations that are just not able to achieve restart, the key factors hindering the separation bubble ingestion can be revealed clearly. For simplicity and clarity, four time instants after diaphragm rupture are displayed, where $t_{cal} = 0$ is defined as the time instant of instantaneous removal of the diaphragm in the simulation. Plotted in Fig. 15 are the mass flow rates calculated at the streamwise stations of interest, such as the cowl lip station C, the geometric throat station T, and the aerodynamic throat stations A_1 or A_2, at the moment when the separation-induced shock moves to its most downstream location during the starting process. Because of the initial flow acceleration by the expansion waves, the mass flow rate at station T increases first, followed by the increase of the mass flow rates at all stations, accompanied with the separation-induced shock moving downstream.

For the inlet with cowl angle of 9°, the mass rates at stations C and A_1 are larger than that at station T until $t_{cal} = 2.17$ ms, when the separation bubble and its induced shock move to their most downstream locations in the internal passage, as seen in Fig. 14(b). After $t_{cal} = 2.17$ ms, the mass flow rate at station A_1 becomes smaller than those at stations C and T, indicating that aerodynamic choking flow appears. Subsequently, the separation bubble and the shock move upstream. As the shock moves out of the cowl lip at $t_{cal} = 2.85$ ms, a rapid decrease in mass flow rate occurs due to inlet spillage, as shown in Fig. 15(b). This result reveals that, for the inlet with cowl angle of 9°, the separation bubble is so large that the aerodynamic throat prevents the separation shock from being swallowed.

For the inlet with cowl angle of 7°, the mass flow rates at stations C, A_1 and A_2 are larger than that at station T during the process that the separation bubble and its induced shock move downstream, as illustrated in Fig. 15(a). The restriction on the flow mass rate at station T prevents the captured air and separation bubbles from moving downstream, first triggers a decrease in mass

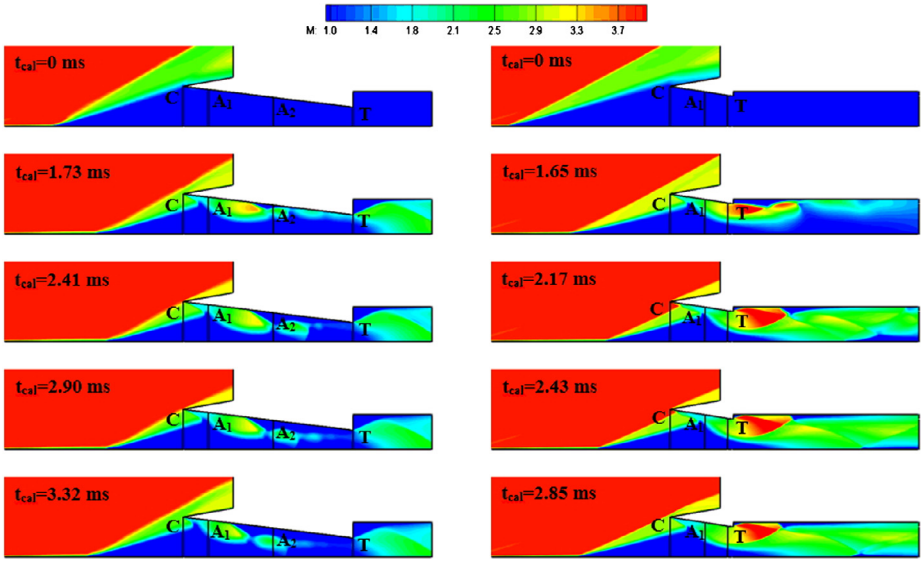

a) α=7°, ICR=2.1 (maximum ICR=1.9) b) α=9°, ICR=1.3 (maximum ICR=1.2)

Fig. 14. Mach contours of starting flow at four time instants after diaphragm rupture.

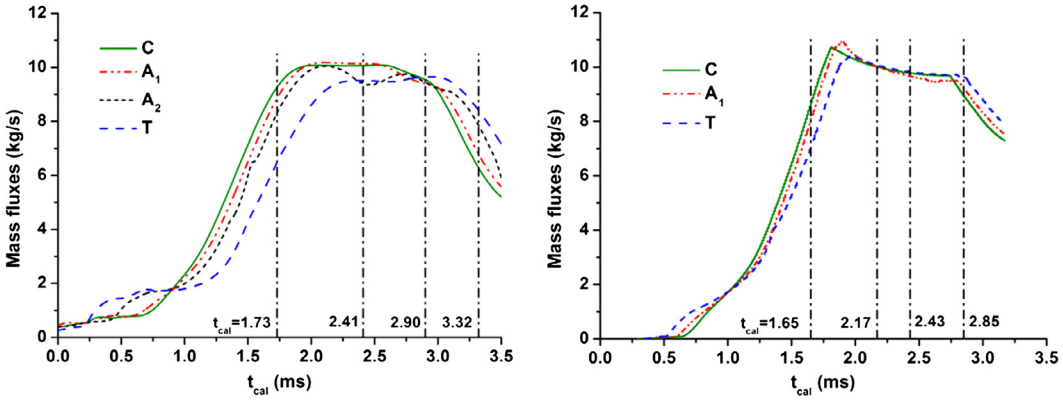

a) α=7°, ICR=2.1 (maximum ICR=1.9) b) α=9°, ICR=1.35 (maximum ICR=1.2)

Fig. 15. Mass flow rates at different stations during the inlet restart process.

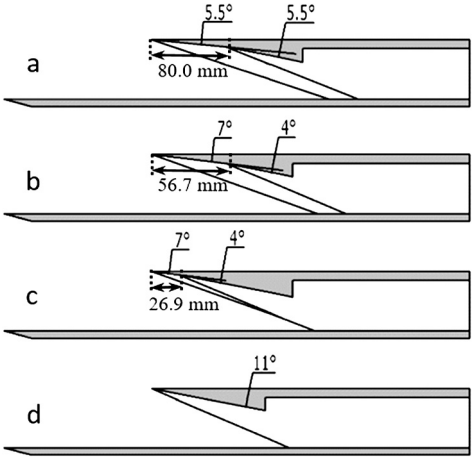

Fig. 16. Sketch of the multiple shocks design with (a) noncoalesced shocks with cowl angle of 5.5° + 5.5°, (b) noncoalesced shocks with cowl angle of 7° + 4°, (c) coalesced shocks with cowl angle of 7° + 4°, and (d) single shock with cowl angle of 11°.

flow rate at station A_2 at $t_{cal} = 2.1$ ms. Subsequently, the mass flow rates at stations A_1 and C drop in turn till $t_{cal} = 2.90$ ms, after which the shock moves out of the cowl lip and gives rise to a rapid drop in mass flow rate due to the inlet spillage. It can be inferred that the geometric throat T chokes the inlet instead of the aerodynamic throat A_1 in the case of the cowl angle of 9°. As a result, the inlet can restart as long as the ICR increases to an extent at which the geometric throat chokes the inlet. Nevertheless, for the cowl angle of 9°, the aerodynamic throat A_1 exerts a dominant impact on the inlet choke although the inlet geometric throat is relatively large. Accordingly, the maximum ICR with the cowl angle of 7° is significantly larger than that of the cowl angle of 9°.

3.5. Design concept of multiple noncoalesced cowl shock waves

Based on the results of the cowl shock effects, a design concept of multiple noncoalesced cowl shock waves was proposed for a large cowl turning angle to improve the inlet restart by reducing the strength of cowl shocks. A total cowl angle of 11° was chosen as an example to verify the effectiveness of multiple cowl shock waves. Cowl configuration with single shock, shown in Fig. 16(d), which can restart at small contraction ratio less than 1.2, has been modified as two configurations with noncoalesced dual shocks, such as 5.5° + 5.5° and 7° + 4°, as illustrated in Fig. 16(a) and Fig. 16(b). To compare with the configuration with noncoalesced dual shocks, a 7° + 4° configuration with coalesced dual cowl shocks was experimentally examined, as shown in Fig. 16(c). The distance from the cowl lip to the second compression corner is 80.0 mm, 56.7 mm and 26.9 mm, respectively.

Fig. 17 shows the experimental results of the four configurations at the cowl lip height H of 30 mm, 40 mm and plate length of 200 mm, 300 mm and 400 mm. It is seen in Fig. 17(a) that Configuration (a) presents the largest inlets restart ICR, and then Configuration (b). Configuration (c) with coalesced shocks does not increase the restart ICR limit because the intersecting shocks lead to almost the same adverse pressure gradient as Configuration (d) with a single shock. For $L = 300$ mm and $H = 40$ mm, compared to the case of Configuration (d) with single shock, the maximum restart ICR increases by 12.5% with Configuration (b) and by 33% with Configuration (a), respectively. In terms of shock strength, the

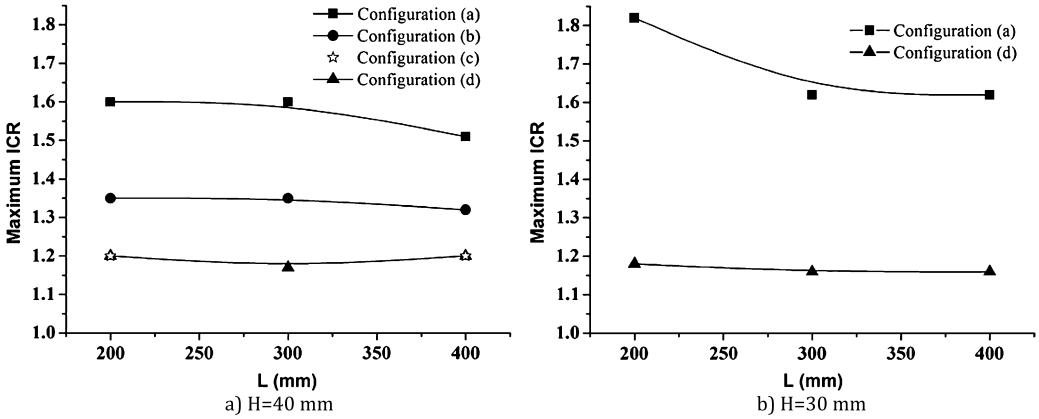

a) H=40 mm b) H=30 mm

Fig. 17. Maximum ICR for different configurations with multiple shocks.

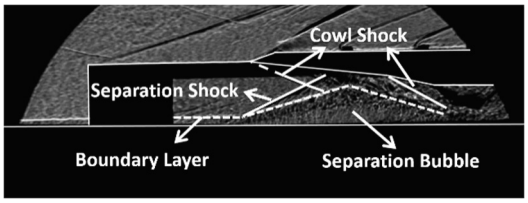

Fig. 18. Schlieren image for Configuration (a) with $H = 40$ mm, $L = 400$ mm.

Table 1
ICR range with transitional pattern.

Configuration (a)	$L = 200$ mm	$L = 300$ mm	$L = 400$ mm
$H = 30$ mm	(1.82–2.00]	(1.62–1.92]	(1.62–2.00]
$H = 40$ mm	(1.60–1.81]	(1.60–1.91]	(1.51–1.95)

shocks are the weakest for Configuration (a), whose corresponding static pressure ratios are 1.70 and 1.62, respectively. Static pressure ratios are 1.94 and 1.42 for Configuration (b). The shock is strongest for Configuration (c), which is almost identical to Configuration (d).

Further comparison between Fig. 17(a) and Fig. 17(b) shows that the configuration (a) gets a slightly higher maximum ICR at the cowl lip height of 30 mm than at the cowl lip height of 40 mm. For the lower cowl lip, the points of noncoalesced cowl shocks impinging on the bottom plate separate farther away from each other. Thus, the interference of two cowl shocks on the plate boundary layer is further weakened and the inlet restart capability is promoted. These results verify that our hypothesis that multiple noncoalesced cowl shocks can significantly benefit the inlet restart by weakening the interaction of cowl shocks with the boundary layer, and can be applied to practical hypersonic inlet designs.

A notable phenomenon is that the transitional restart pattern occurs at a wider range of ICR for all conditions of Configuration (a) compared to the single shock configuration. A typical schlieren image is shown in Fig. 18 and the corresponding ICR range is shown in Table 1. The hysteresis of boundary layer separation is suspected to be responsible for this phenomenon. Especially, the adverse pressure gradient induced by downstream shock prevents the separation bubble from moving downstream. The underlying mechanism of the separation evolvement merits further detailed study in the future and will not be considered in the present study. If the transitional pattern can be turned into restart mode, the inlet restart capability will be significantly improved.

4. Concluding remarks

An experimental study was conducted in the GJF shock tunnel to investigate the restart characteristics of simple ramp type hypersonic inlets with thin boundary layers at the freestream Mach number of 4.0, emphasizing on the effect of the cowl shock. To examine the inlet restart within the short duration of the GJF shock tunnel, a test method was adopted by employing the controllable diaphragm rupture technique. A set of cowl configurations with different internal contraction ratios (ICR) were tested to obtain the maximum ICR allowing the inlet restart for various cowl angles, cowl lip heights, and plate lengths. The inlet unstart/restart behaviors were visualized by high-speed schlieren images together with the static pressure measurement.

Other than the restarted and un-restarted inlet flow patterns, a transitional mode was identified as that the mass capture is the same as that of the started inlet while a larger separation bubble with an associated shock stays in the internal passage. Such an inlet mode cannot be deemed as started due to its large separation loss. Consequently, the restarted mode was identified in the present study as the case in which all the pressures and schlieren images resemble those without diaphragm.

The present study shows that the cowl shock plays a dominant role in the inlet restart. A stronger cowl shock tends to degrade the inlet restart capability because of the larger separation bubble and the higher pressure loss during the starting process. The maximum ICR can vary between 1.2 and 2.1 for different cowl angles, significantly different from the Kantrowitz limit. In addition, we experimentally determined a sensitive range of the cowl angles, 7°–9°, within which the restart contraction ratio decreases rapidly because the geometric throat controlling the mass flow rate at relatively small angles is transitioned to the aerodynamic throat at larger angles. Accordingly, a design concept of multiple noncoalesced cowl shocks was proposed and verified for its capability of significantly improving the inlet restart. The present experimental results are expected to be useful for characterizing and designing the hypersonic inlets in the future.

Conflict of interest statement

The authors declare that there is no conflict of interests regarding the publication of this article.

Acknowledgements

The work in the Institute of Mechanics, Chinese Academy of Sciences was supported by the National Natural Science Foundation of China (Grant No. 11472279 and 11672309). The work in the Hong Kong Polytechnic University was supported by the Hong Kong Polytechnic University Central Research Grants (G-UA2M and G-YBGA). The collaboration between the two institutions was additionally supported by the “Open Fund” of State Key Laboratory of High-Temperature Gas Dynamics, Chinese Academy of Sciences.

References

[1] Z.F. Li, W.Z. Gao, H.L. Jiang, J.M. Yang, Unsteady behaviors of a hypersonic inlet caused by throttling in shock tunnel, AIAA J. 51 (10) (2013) 2485–2492.
[2] J. Chang, N. Li, K. Xu, W. Bao, D. Yu, Recent research progress on unstart mechanism, detection and control of hypersonic inlet, Prog. Aerosp. Sci. 89 (2017) 1–22.
[3] D. Mahapatra, G. Jagadeesh, Studies on unsteady shock interactions near a generic scramjet inlet, AIAA J. 47 (9) (2009) 2223–2232.
[4] X. Jiao, J. Chang, Z. Wang, D. Yu, Mechanism study on local unstart of hypersonic inlet at high Mach number, AIAA J. 53 (10) (2015) 3102–3112.
[5] A. Kantrowitz, C. Donaldson, Preliminary Investigation of Supersonic Diffusers, NACA ACR-L5D20, May 1945.
[6] A. Kantrowitz, The Formation and Stability of Normal Shock Waves in Channel Flows, NACA TN 1225, March 1947.
[7] S. Mölder, E.V. Timofeev, R.B. Tahir, Flow starting in high compression hypersonic air inlets by mass spillage, in: 40th AIAA/ASME/SAE/ASEE Joint Propulsion Conference and Exhibit, July 2004, AIAA Paper 2004-4130.
[8] A. Najafiyazdi, R.B. Tahir, E.V. Timofeev, S. Mölder, Analytical and numerical study of flow starting in supersonic inlets by mass spillage, in: 43rd AIAA/ASME/SAE/ASEE Joint Propulsion Conference and Exhibit, July 2007, AIAA Paper 2007-5122.
[9] X. Veillard, R.B. Tahir, E.V. Timofeev, S. Mölder, Limiting contractions for starting simple ramp-type scramjet intakes with overboard spillage, J. Propuls. Power 24 (5) (2008) 1042–1049.
[10] D.M.V. Wie, Scramjet propulsion, in: E.T. Curran, S.N.B. Murthy (Eds.), Scramjet Propulsion, in: Prog. Astronaut. Aeronaut., vol. 189, AIAA, Reston, VA, 2000, pp. 462–465.
[11] M.K. Smart, Experimental testing of a hypersonic inlet with rectangular-to-elliptical shape transition, J. Propuls. Power 17 (2) (2001) 276–283.
[12] Y. Wang, Z.G. Wang, J.H. Liang, X.Q. Fan, Investigation on hypersonic inlet starting process in continuous freejet wind tunnel, J. Propuls. Power 30 (6) (2014) 1721–1726.
[13] T.J. Goldberg, J.N. Hefner, Starting criterion for hypersonic inlets, J. Aircr. 7 (3) (1970) 275–277.
[14] T.J. Goldberg, J.N. Hefner, Starting Phenomena for Hypersonic Inlet with Thick Turbulent Boundary Layers at Mach 6, NASA TN D-6280, August 1971.
[15] R.J. McGregor, S. Mölder, T.W. Paisley, Hypersonic inlet flow starting in the Ryerson University of Toronto gun tunnel, in: Investigations in the Fluid Dynamics of Scramjet Inlets, Ryerson Polytechnical University and the University of Toronto, Canada, 1992, pp. 4.1–4.50.

[16] D.M.V. Wie, F.T. Kwok, R.F. Walsh, Starting characteristics of supersonic inlets, in: 32nd AIAA/ASME/SAE/ASEE Joint Propulsion Conference and Exhibit, July 1996, AIAA Paper 1996-2914.

[17] A.K. Flock, A. Gülhan, Experimental investigation of the starting behavior of a three-dimensional scramjet intake, AIAA J. 53 (9) (2015) 2686–2693.

[18] J. Chang, D. Yu, W. Bao, Effects of boundary-layers bleeding on unstart/restart characteristics of hypersonic inlets, Aeronaut. J. 113 (1143) (2009) 319–327.

[19] J. Chang, Y. Fan, Effects of boundary layers bleeding on performance parameters of hypersonic inlets, Aircr. Eng. Aerosp. Technol. 81 (3) (2009) 204–211.

[20] R.B. Tahir, S. Mölder, Unsteady starting of high Mach number air inlets – a CFD study, in: 39th AIAA/ASME/SAE/ ASEE Joint Propulsion Conference and Exhibit, July 2003, AIAA Paper 2003-5191.

[21] H. Ogawa, A.L. Grainger, R.R. Boyce, Inlet starting of high-contraction axisymmetric scramjets, J. Propuls. Power 26 (6) (2010) 1247–1258.

[22] E.V. Timofeev, R.B. Tahir, S. Mölder, On recent developments related to flow starting in hypersonic air intakes, in: AIAA International Space Planes and Hypersonic Systems and Technologies Conference, May 2008, AIAA Paper 2008-2512.

[23] J. Teng, H.C. Yuan, Variable geometry cowl sidewall for improving rectangular hypersonic inlet performance, Aerosp. Sci. Technol. 42 (2015) 128–135.

[24] H. Liu, L.J. Yue, Y.B. Xiao, H. Peng, X.Y. Chang, Experimental Method for Hypersonic Inlet Self-Starting in Shock Tunnel, AJCPP 2012-173, Oct. 2012.

[25] H.J. Tan, S. Sun, Z.L. Yin, Oscillatory flows of rectangular hypersonic inlet unstart caused by downstream mass-flow choking, J. Propuls. Power 25 (1) (2009) 138–147.

[26] H.J. Tan, L.G. Li, Y.F. Wen, Q.F. Zhang, Experimental investigation of the unstart process of a generic hypersonic inlet, AIAA J. 49 (2) (2011) 279–288.

[27] D.R. Chapman, D.M. Kuehn, H.K. Larson, Investigation of Separated Flows in Supersonic and Subsonic Streams with Emphasis on the Effect of Transition, NACA Rep. 1356, 1958.

[28] Z.G. Wang, Y.L. Zhao, Y.X. Zhao, X.Q. Fan, Prediction of massive separation of unstarted inlet via free-interaction theory, AIAA J. 53 (4) (2015) 1108–1111.

[29] E.E. Zhukoski, Turbulent boundary-layer separation in front of a forward-facing step, AIAA J. 5 (10) (1967) 1746–1753.

[30] H.B. Lu, L.J. Yue, X.Y. Chang, Flow characteristics of hypersonic inlets with different cowl-lip blunting methods, Sci. China, Phys. Mech. Astron. 57 (4) (2014) 741–752.

[31] H.B. Lu, L.J. Yue, Y.B. Xiao, X.Y. Zhang, Interaction of isentropic compression waves with a bow shock, AIAA J. 51 (10) (2013) 2474–2484.